Grey wolf optimization tuned drivetrain vibration controller with backlash compensation strategy using time-dependent-switched Kalman filter

Heisei Yonezawa[#1], Ansei Yonezawa[#2], Itsuro Kajiwara [#3]

#1(Corresponding author)
Division of Mechanical and Aerospace Engineering, Hokkaido University
N13, W8, Kita-ku, Sapporo 060-8628, Japan
Phone +81-80-4039-9406
E-mail: yonezawah@eng.hokudai.ac.jp

#2
Division of Mechanical and Aerospace Engineering, Hokkaido University
N13, W8, Kita-ku, Sapporo 060-8628, Japan
Phone +81- 90-2893-3160
E-mail: ayonezawa@eng.hokudai.ac.jp

#3
Division of Mechanical and Aerospace Engineering, Hokkaido University
N13, W8, Kita-ku, Sapporo 060-8628, Japan
Phone +81-11-706-6390, Fax. +81-11-706-6390
E-mail: ikajiwara@eng.hokudai.ac.jp

Abstract

To improve the performance and durability of vehicle components, efforts have been made to reduce driveline oscillations using advanced active control algorithms. However, existing methods often rely on subjective parameter adjustments, which can be burdensome for designers. This study introduces an effective tuning algorithm for a driveline vibration controller that accounts for nonlinear backlash effects. Initially, a driveline dynamics model is developed to focus on transient oscillations resulting from changes in driving force and the presence of nonlinear backlash. The backlash impact is incorporated into the model through a discontinuous dead-zone region. Two operational dynamics, which are the *contact mode* and the *backlash mode*, are considered. A dynamic output feedback H_2 controller is designed as a baseline controller to mitigate low-frequency resonance in the driveline. A solution for managing the nonlinear backlash challenges is introduced, involving the use of a simple control mode switching algorithm in conjunction with the controller. This algorithm relies on a time-dependent-switched Kalman filter. Additionally, the optimal settings for the parameters needed by the mode-switching algorithm are autonomously determined using the grey wolf optimizer (GWO). The proposed active controller can be implemented in real vehicles by using an on-vehicle acceleration sensor and electronic control unit (ECU). In a simulation environment, the vehicle body vibration is online fed back to the resultant controller, and an actuator is supposed to apply control commands to the driveline. The effectiveness of this newly proposed active controller is confirmed through comparative tests, revealing the superior vibration control.

Keywords: Active vibration control, Drivetrain, Nonlinear backlash, Kalman filter, Grey wolf optimization, Robustness analysis

1. Introduction

1.1. Motivation and related work: Active driveline vibration control

Given the recent shift towards reducing size, cutting weight, enhancing comfort, and achieving high performance, the significance of vibration control technology has grown more apparent.[1,2,3] Vibration control is also a crucial technology in automotive powertrains. Sudden changes in driving torque can lead to temporary vibrations in the driveline of a vehicle,[4] which can seriously affect both comfort and the lifespan of components. Active vibration control has proven to be an effective solution. For instance, methods like adaptive disturbance observation,[5] adaptive active control,[6] and model-reference adaptive linear quadratic tracking controllers have been successfully employed to minimize vehicle oscillations.[7] The main contribution of the above works was to demonstrate that the advanced control algorithms can be implemented in a driveline control system with various mechanical limitations and are applicable to the active damping to improve the drivability and comfortability. For instance, one study coped with the time-varying feature due to an engine mechanism.[5] On the other hand, their common shortcoming is that the control methods mentioned above fail to account for the nonlinear backlash.

1.2. Related work: Driveline vibration controller considering backlash

Backlash leads to an increase in oscillation amplitude.[8,9] This phenomenon arises within the gear mechanism of the driveline. Backlash introduces a discontinuous shift between two operational dynamics: the *contact mode,* where a mechanical connection exists throughout the driveline, and the *backlash mode,* where the motor and wheel sides become decoupled because of clearance issues. This nonlinearity presents a challenging problem, making it difficult to design an active control system with high performance.

Several methods have been documented for managing driveline oscillation and considering the issue of backlash. These methods encompass a robust disturbance observer-oriented strategy[10] and the utilization of sliding mode control techniques.[11,12]

One of the most logical concepts involves the transition of control systems based on the presence of contact or backlash mode. As the illustrative instance, the concurrent implementation of a proportional-integral-differential controller and a linear-quadratic regulator (LQR) has been realized.[13] The contribution of other related works[9,14] was to construct a control algorithm centered on mode-switching, contingent upon the establishment of a threshold value for vehicle jerk to alleviate the repercussions of backlash. However, there are still shortcomings within the above approaches as follows:

- Previous research lacks an efficient method for optimizing various design parameters necessary for controlling driveline oscillations while accounting for backlash.
- A backlash compensation strategy should be simpler and more systematic, requiring fewer online calculations. For the previous strategy,[9,14] the setting of the effective threshold is not always easy due to the absence of a clear design policy and the requirement of prior information on vehicle jerk.

1.3. Related work: Optimization algorithm-based controller for powertrain

As widely recognized, optimization algorithms are commonly employed to effectively produce suitable solutions for addressing feedback control challenges.[15] Several studies have proposed the concept of framing powertrain dynamics control as optimization tasks.[16,17,18] These publications have hinted at the significance of iterative offline simulations involving powertrain models and the need to incorporate efficient optimization algorithms.

Among the various methods used for controlling a driveline, some important works developed a torque shaping controller to reduce the jarring impact due to the occurrence of clunk in backlash. The contribution by this controller is to ensure a smooth response when passing through backlash.[8,19] Another study revealed that genetic algorithm is applicable to find the ideal weighting coefficients necessary for designing an LQR vibration controller.[20] More recently, the utilization of Bayesian optimization has been proposed positively.[21] Many researchers have opted for a model predictive control (MPC) approach.[22] MPC offers the advantage of determining optimal control commands in real-time while effectively addressing limitations. However, the previous studies mentioned still have the following shortcomings.

- The shortcomings include overlooking the nonlinearity caused by backlash, not incorporating intelligent optimization algorithms for crucial controller parameters like the contact mode controller, and the need for computationally intensive online tasks.
- For the existing works, there is a demand for a simpler approach to compensate for backlash.

1.4. Contribution and novelty of this study

To address the above challenges remaining in the previous works, this paper introduces an automated tuning method for a driveline vibration controller that considers the nonlinear behavior of backlash. This approach newly utilizes the grey wolf optimizer (GWO) and represents an advancement over our prior research efforts,[9] where we manually fine-tuned the essential control parameters through trial-and-error experimentation. In this paper, we propose a simple control mode switching for the backlash compensation algorithm based on the contact and backlash modes. The novel advancement is to guarantee the successful transition between the two modes by introducing a time-dependent-switched linear Kalman filter (TDSLKF). The intended algorithm seeks to effectively reduce the low-frequency resonance in a driveline while also mitigating the disruptive effects of the backlash mode.

Below, we outline the key contributions of this paper.

(C1). Compared to the existing related works,[9,13,14,20] the new contribution of this study is to develop an automated tuning approach based on GWO[23] for actively controlling driveline oscillations while compensating for backlash.

(C2). The simpler mode-switching algorithm is constructed to handle the nonlinear backlash. The advantage over the previous approach[9] is that the mode switching is ensured in a more systematic manner based on the TDSLKF.

(C3). The suggested method is examined through comparative simulations using a driveline dynamics model. We assess the resilience to variations in driveline dynamics and find the dominance given by GWO and TDSLKF over the existing methods.[9,14]

2. Driveline system with nonlinear backlash

2.1. Driveline model

The driveline model presented in this section, which builds upon our previous research,[9,14,24] is depicted in Fig. 1(a). It serves as a simplified representation of an actual automobile driveline and is primarily designed to examine transient oscillations resulting from sudden changes in driving force and the presence of nonlinear backlash. The parameter values of the model can be found in Table 1. The impact of backlash is incorporated into the model through a discontinuous dead-zone region.

While the driveline model presented in this paper can reproduce only the basic configuration of a real vehicle driveline, the other detailed parts are simplified in order to focus on the effect due to the backlash. In other words, the model does not correspond exactly to all the details of a real vehicle driveline. This is because it is necessary to make it easier to evaluate the efficacy of a control strategy for the backlash by omitting other detailed elements of a real vehicle. On the other hand, the simplified driveline model is sufficient to capture only the basic structure of actual driveline dynamics. M_E corresponds to inertia of the actuator, m_G represents the intermediate part, and M_B corresponds to the vehicle body. These parts are connected via rigidity and damping, which correspond to those of the drive shaft and so on. Of particular importance is that the dead-zone of backlash is set at the location that takes into account that of a real driveline. Therefore, the phenomenon caused by the backlash is explicitly reflected in the model. Upon considering the structure of a real vehicle, the validity of this model has already been acknowledged in previous studies.[9,24,25] For a more comprehensive understanding of this model, additional details are provided in our previous works.[9,25]

Fig. 1(b) illustrates two distinct modes of driveline dynamics. The first mode, known as the contact mode, enables the coupling of the driven side M_E with the output side M_B, which includes the actuator and the vehicle body. In the second mode, referred to as the backlash mode, these two components are forcibly separated because of clearance traversal.

Table 1 Parameter values and descriptions of the driveline

Parameter	Description	Value	Unit
K_C	Spring connected with M_B	660.0	N/m
K_G	Spring between M_E and m_G	5.3×10^4	N/m
K_D	Spring between M_B and m_G	2.2×10^4	N/m
M_E	Mass of the actuator	1.04	kg
m_G	Mass of the intermediate part	0.039	kg
M_B	Mass of the vehicle body	0.232	kg
C_D	Damper between M_B and m_G	12.5	Ns/m
C_C	Damper connected with M_B	0.1	Ns/m
C_{cl}	Damper of M_E	1.5	Ns/m
C_G	Damper between M_E and m_G	36.0	Ns/m

2.2. State-space representation

In order to obtain a fundamental oscillation controller, the initial step involves obtaining the linearized model from the driveline dynamics, considering non-linear factors like backlash. Previous research has already formulated the time-varying linear state equation for the plant model[9,26]:

$$\dot{\boldsymbol{x}}_d = \boldsymbol{A}_d\boldsymbol{x}_d + \boldsymbol{B}_{d1}\boldsymbol{w}_d + \boldsymbol{B}_{d2}u \tag{1}$$

$$y_d = \boldsymbol{C}_d\boldsymbol{x}_d + \boldsymbol{D}_{d1}\boldsymbol{w}_d + D_{d2}u \tag{2}$$

$$\boldsymbol{A}_d = \begin{bmatrix} 0 & 0 & 0 & 1 & 0 & 0 \\ 0 & 0 & 0 & 0 & 1 & 0 \\ 0 & 0 & 0 & 0 & 0 & 1 \\ -\frac{(K_D + K_C)}{M_B} & \frac{K_D}{M_B} & 0 & -\frac{(C_D + C_C)}{M_B} & \frac{C_D}{M_B} & 0 \\ \frac{K_D}{m_G} & -\frac{(SwK_G + K_D)}{m_G} & \frac{SwK_G}{m_G} & \frac{C_D}{m_G} & -\frac{(SwC_G + C_D)}{m_G} & \frac{SwC_G}{m_G} \\ 0 & \frac{SwK_G}{M_E} & -\frac{SwK_G}{M_E} & 0 & \frac{SwC_G}{M_E} & -\frac{(SwC_G + C_{cl})}{M_E} \end{bmatrix}$$

$$\boldsymbol{B}_{d1} = \begin{bmatrix} 0 & 0 \\ 0 & 0 \\ 0 & 0 \\ 0 & \frac{1}{M_B} \\ \frac{1}{m_G} & 0 \\ -\frac{1}{M_E} & 0 \end{bmatrix}, \quad \boldsymbol{B}_{d2} = \begin{bmatrix} 0 \\ 0 \\ 0 \\ 0 \\ 0 \\ \frac{1}{M_E} \end{bmatrix} \tag{3}$$

$$\boldsymbol{C}_d = [1 \quad 0 \quad 0 \quad 0 \quad 0 \quad 0]$$

$$\boldsymbol{D}_{d1} = 0, \quad D_{d2} = 0$$

$$\boldsymbol{x}_d = [X_B \quad x_G \quad X_E \quad \dot{X}_B \quad \dot{x}_G \quad \dot{X}_E]^T \tag{4}$$

u represents the control input, while $\boldsymbol{w}_d$ indicates disturbances, including the force stemming from backlash. The parameter Sw is crucial in describing the impact of the dead-zone effect caused by backlash. Eq. (5) illustrates the switching rule.[27,28] $|\delta|$ signifies the width of the dead zone, and F represents the force exerted by the stiffness K_G. When developing a baseline controller, Sw is assigned a value of 1.0.

$$
\begin{aligned}
&F = OKG + Sw \cdot K_G \cdot \Delta X, \quad \Delta X = X_E - x_G \\
&Sw = \begin{cases} 1, & \Delta X > |\delta| \\ 1, & \Delta X < -|\delta| \\ 0, & |\Delta X| \leq |\delta| \end{cases} \\
&OKG = \begin{cases} 0, & |\Delta X| \leq |\delta| \\ -\left|K_G \times |\delta|\right|, & \Delta X > |\delta| \\ \left|K_G \times |\delta|\right|, & \Delta X < -|\delta| \end{cases}
\end{aligned}
\tag{5}
$$

The plant model in the previous work[9] is also detailed, including its time-dependent linear state equation, which incorporates features like backlash and other nonlinear traits.

3. Active reduction of oscillations while compensating for backlash

Fig. 2 illustrates the setup of the active control system. This system effectively addresses both contact mode and backlash mode issues.

3.1. Output feedback H_2 vibration controller

The fundamental controller is formulated as an H_2 output feedback approach[29,30] to explicitly assess the driveline transient oscillations. In the block diagram depicted in Fig. 3(a), which serves as the foundation for deriving the controller, we minimize the H_2 norm $||T_{zw}(s)||_2^2$ of the transfer function $T_{zw}(s)$ from w (i.e., external input) to $z = [z_y \quad z_u]^T$ (i.e., controlled variables). The expanded plant $G(s)$, which encompasses the controlled system $P_c(s)$, a high pass filter denoted as $W_{Highpass}$, and a low-pass filter named $W_{Lowpass}$, is designed to confine the effective control frequency range of the vibrations of the vehicle body to a lower-frequency spectrum.[9,26] This design process is executed using the Control System Toolbox and Robust Control Toolbox in MATLAB.

The parameters Q_i and R_i are crucial weighting constants that necessitate meticulous tuning. Here, i represents the iteration count for the latter optimization phase. z_y and

z_u correspond to the amplifications of the vehicle vibration signal y_G and the control input signal u_G from the expanded plant, respectively, and are determined by the values of Q_i and R_i, as illustrated below:

$$z_y = \sqrt{Q_i} \cdot y_G \tag{6}$$

$$z_u = \sqrt{R_i} \cdot u_G \tag{7}$$

The choice of Q_i and R_i has an impact on the level of oscillation performance, as discussed in the related works.[20,26] If a higher degree of vibration suppressions is needed, it is advisable to increase the value of Q_i. Conversely, increasing the values of R_i promotes energy-efficient control and places greater emphasis on robust stability. These values were determined through manual and subjective methods in our prior research.[26]

3.2. Mode switching strategy based on TDSLKF

To mitigate the effects of backlash on the body of the vehicle, the compensation strategy, which switches the control modes illustrated in Fig. 3(b), is integrated with the H_2 oscillation controller.[9,12,14] The objective of the backlash mode control is to facilitate a rapid transition from negative contact to positive contact while minimizing the impact when the backlash transition concludes with a gentle landing.

During the contact mode, the discretized state equation $(\boldsymbol{A}_{Ki}, \boldsymbol{B}_{Ki}, \boldsymbol{C}_{Ki}, D_{Ki})$ of the H_2 controller is typically executed according to Eqs. (8)-(10).

In the context of the control method described in Eqs. (11)-(15) for dealing with backlash, a modification is made to the reference signal $R(k)$ sent to the H_2 controller. This modified reference signal, denoted as R_i^{BL}, serves the purpose of guiding the controller to produce a controlled input that smoothly navigates through the backlash while ensuring a gentle landing when it concludes. At the same time, a compensation mechanism called anti-windup is employed. Anti-windup temporarily suspends the updating of the state vector $\boldsymbol{x}_K(k)$ defined by $(\boldsymbol{A}_{Ki}, \boldsymbol{B}_{Ki}, \boldsymbol{C}_{Ki}, D_{Ki})$, to prevent the accumulation of control errors caused by the dead-zone effect of the backlash. In Eq. (12), the term z^{-1} represents an operator that introduces a one-control cycle delay, effectively implementing the anti-windup. As a result, excessive and unnecessary large control inputs during the backlash mode are minimized, contributing to a smoother landing. Further details about this compensation approach can be found in our previous works.[9,14,26]

It is worth noting that both the backlash mode and contact mode controls are executed using a single H_2 controller. This simple setup eliminates the need for designing multiple controllers specialized for managing mode switches.

(Contact mode control):

$$\boldsymbol{x}_K(k+1) = \boldsymbol{A}_{Ki}\boldsymbol{x}_K(k) + \boldsymbol{B}_{Ki}E(k) \tag{8}$$

$$U_{CO}(k) = \boldsymbol{C}_{Ki}\boldsymbol{x}_K(k) + D_{Ki}E(k) + K_C R(k) \tag{9}$$

$$E(k) = R(k) - X_B(k) \tag{10}$$

(Backlash mode control):

$$\boldsymbol{x}_{AW}(k+1) = \boldsymbol{A}_{Ki}\boldsymbol{x}_K(k) + \boldsymbol{B}_{Ki}E_{BL}(k) \tag{11}$$

$$\boldsymbol{x}_{AW}(k) = z^{-1}[\boldsymbol{x}_{AW}(k+1)] \quad (\,\boldsymbol{x}_{AW}(k) = \boldsymbol{x}_K(k)\,) \tag{12}$$

$$\boldsymbol{x}_K(k+1) = \boldsymbol{x}_{AW}(k) \quad \text{i.e., Substitute } \boldsymbol{x}_{AW}(k) \text{ for } \boldsymbol{x}_K(k+1) \tag{13}$$

$$U_{BL}(k) = \boldsymbol{C}_{Ki}\boldsymbol{x}_K(k) + D_{Ki}E_{BL}(k) + K_C R_i^{BL} \tag{14}$$

$$E_{BL}(k) = R_i^{BL}(k) - X_B(k) = R_i^{BL} - X_B(k) \tag{15}$$

In order to transition between the two control modes, it is essential to know when the backlash has been fully crossed. This research employs TDSLKF[31] to estimate this crucial moment, ensuring a smooth transition from the backlash mode to the contact mode. ΔT_s represents the sampling time, and the Kalman filtering process progresses as outlined in Eqs. (16)-(20).

(A priori estimate):

$$\begin{aligned}\hat{\boldsymbol{x}}_{dd}{}^{-}[k] &= \{\boldsymbol{I}_{6\times 6} + \Delta T_s \boldsymbol{A}_d((k-1)\Delta T_s)\}\hat{\boldsymbol{x}}_{dd}[k-1] \\ &+\Delta T_s[\boldsymbol{B}_{d1}((k-1)\Delta T_s) \quad \boldsymbol{B}_{d2}((k-1)\Delta T_s)]\begin{bmatrix}\boldsymbol{w}_d[k-1] \\ u[k-1]\end{bmatrix}\end{aligned} \tag{16}$$

(A priori covariance matrix):

$$\begin{aligned}&\boldsymbol{P}^{-}[k] \\ &= \{\boldsymbol{I}_{6\times 6} + \Delta T_s \boldsymbol{A}_d((k-1)\Delta T_s)\}\boldsymbol{P}[k-1]\{\boldsymbol{I}_{6\times 6} + \Delta T_s \boldsymbol{A}_d((k-1)\Delta T_s)\}^T \\ &+(\Delta T_s)^2[\boldsymbol{B}_{d1}((k-1)\Delta T_s) \quad \boldsymbol{B}_{d2}((k-1)\Delta T_s)]\boldsymbol{Q}\begin{bmatrix}\boldsymbol{B}_{d1}^T((k-1)\Delta T_s) \\ \boldsymbol{B}_{d2}^T((k-1)\Delta T_s)\end{bmatrix}\end{aligned} \tag{17}$$

(Kalman gain):

$$\boldsymbol{g}[k] = \boldsymbol{P}^{-}[k]\boldsymbol{C}_{dd}^T[k](\boldsymbol{C}_{dd}[k]\boldsymbol{P}^{-}[k]\boldsymbol{C}_{dd}^T[k] + \boldsymbol{R})^{-1} \tag{18}$$

(Estimated state variable):

$$\hat{\boldsymbol{x}}_{dd}[k] = \hat{\boldsymbol{x}}_{dd}{}^{-}[k] + \boldsymbol{g}[k]\{\boldsymbol{y}_{dd}[k] - \boldsymbol{C}_{dd}[k]\hat{\boldsymbol{x}}_{dd}{}^{-}[k]\} \tag{19}$$

(A posteriori covariance matrix):

$$\boldsymbol{P}[k] = \{\boldsymbol{I}_{6\times6} - \boldsymbol{g}[k]\boldsymbol{C}_{dd}[k]\}\boldsymbol{P}^{-}[k] \tag{20}$$

In TDSLKF, the covariance matrices $\boldsymbol{Q}$ and $\boldsymbol{R}$ of system and observation noises and the observed output $\boldsymbol{y}_{dd}[k]$ are defined as

$$\boldsymbol{Q} = 1.0\times10^{9}\boldsymbol{I}_{3\times3},\ \boldsymbol{R} = \begin{cases} 1.0\times10^{3}\boldsymbol{I}_{1\times1} & (Sw=1) \\ 1.0\times10^{3}\boldsymbol{I}_{2\times2} & (Sw=0) \end{cases} \tag{21}$$

$$\boldsymbol{y}_{dd}[k] = \begin{cases} X_B(k\Delta T_s) & (Sw=1) \\ \begin{bmatrix} X_B(k\Delta T_s) \\ X_E(k\Delta T_s) \end{bmatrix} & (Sw=0) \end{cases} \tag{22}$$

$$\boldsymbol{C}_{dd}[k] = \begin{cases} \begin{bmatrix} 1 & 0 & 0 & 0 & 0 & 0 \end{bmatrix} & (Sw=1) \\ \begin{bmatrix} 1 & 0 & 0 & 0 & 0 & 0 \\ 0 & 0 & 1 & 0 & 0 & 0 \end{bmatrix} & (Sw=0) \end{cases} \tag{23}$$

The parameter Sw is computed using Eq. (5) and components $\hat{X}_E[k]$ and $\hat{x}_G[k]$ in the estimated state vector $\hat{\boldsymbol{x}}_{dd}[k]$.

$$\hat{\boldsymbol{x}}_{dd}[k] = \begin{bmatrix} \hat{X}_B[k] & \hat{x}_G[k] & \hat{X}_E[k] & \hat{\dot{X}}_B[k] & \hat{\dot{x}}_G[k] & \hat{\dot{X}}_E[k] \end{bmatrix}^T \tag{24}$$

According to $\hat{\boldsymbol{x}}_{dd}[k]$ in Eq. (24), we can identify whether a driveline system is in the backlash mode or the contact mode. The estimation algorithm for Control mode is simply given by Eq. (25).

$$\text{Control mode} = \begin{cases} \text{Backlash mode, if } \hat{X}_E[k] - \hat{x}_G[k] \le |\delta| \\ \text{Return to Contact mode, if } \hat{X}_E[k] - \hat{x}_G[k] > |\delta| \end{cases} \tag{25}$$

In the previous studies,[9,14,26] the estimation for the driveline's dynamics modes has relied on a threshold value for vehicle jerk. This is simple; however, setting an effective threshold is not always easy due to the absence of its clear design policy as well as the requirement of prior information on vehicle jerk. Compared to the previous threshold-based algorithm, the TDSLKF-based estimation has a systematic manner, which does not demand prior information on jerk.

Be aware that the crucial factor for the success of the compensation mentioned above lies in the soft-landing reference R_i^{BL}. Excessively high values of R_i^{BL} result in a failure to achieve a gentle landing, whereas extremely small values of R_i^{BL} cause a decline in responsiveness. Determining an appropriate R_i^{BL} value has proven to be a difficult and onerous task, requiring designers to engage in manual trial-and-error procedures.[9,26]

4. GWO-based automatic tuning scheme for active control system

4.1. Grey wolf optimizer[23]

The proposed tuning approach utilizes the GWO[23] because of the necessity of few hyperparameters, leading to simplicity. GWO is a powerful swarm-intelligence-based metaheuristic algorithm and has been used in a wide variety of engineering problems[32] such as control system optimizations[33] due to its capability of searching for a global solution in a simple and systematic manner. For example, one study applied GWO to optimization of a fuzzy logic-based active vibration controller for seismically excited building structures.[34] For a sun-tracker system, an optimal tuning approach of a fuzzy controller was proposed.[35] Recently, tuning with GWO for a PID controller has been studied. Such examples include various control issues such as magnetic levitation systems.[36] The above review clearly indicates the effectiveness and validity of applying GWO to tuning problems of feedback control systems.

This algorithm emulates the natural social dominant hierarchy of grey wolves and takes inspiration from their pack hunting technique for its search process.

Grey wolves exhibit a rigid social hierarchy within their packs, as illustrated in Fig. 4(a).

They are divided into four distinct classes characterized by their hierarchical dominance.[23] The upper three levels, specifically the alpha, beta, and delta wolves, assume leadership roles because of their superior capabilities in guiding the pack. These three leaders play a pivotal role in directing hunting efforts, akin to optimization processes. It is assumed that the alpha, beta, and delta wolves guide the rest of the pack towards locating prey. On the other hand, the lowest level comprises the omega wolves, who hold subordinate positions and follow the guidance provided by the leaders.

The cooperative hunting strategy employed by grey wolves involves three primary phases: first, they seek out their prey by tracking it; then, they encircle the prey until it stops its movements; finally, they initiate the attack by approaching their target. One especially distinctive aspect of this hunting process is the encircling maneuver executed by each individual wolf. To describe this encircling behavior mathematically, an update to the position of each wolf has been devised, considering the position of the prey, as outlined below:

$$\boldsymbol{D} = \left|\boldsymbol{C} \cdot \boldsymbol{X}_p(i) - \boldsymbol{X}(i)\right| \tag{26}$$

$$\boldsymbol{X}(i+1) = \boldsymbol{X}_p(i) - \boldsymbol{A} \cdot \boldsymbol{D} \tag{27}$$

$$\boldsymbol{A} = 2a \cdot \boldsymbol{r}_1 - a \tag{28}$$

$$\boldsymbol{C} = 2 \cdot \boldsymbol{r}_2 \tag{29}$$

The index i in the context represents the ith iteration. $\boldsymbol{X}(i)$ and $\boldsymbol{X}_p(i)$ denote the position vectors of individual wolves (referred to as search agents) and the prey (the optimal solution), for the ith iteration, respectively. Additionally, $\boldsymbol{r}_1 \in [0, 1]$ and $\boldsymbol{r}_2 \in [0, 1]$ are random variables, serving to introduce randomness into the algorithm. $\boldsymbol{A}$ is a coefficient vector to guarantee smooth transition from exploration to exploitation in the optimization process. $\boldsymbol{C}$ represents a random vector of coefficients designed to promote exploration and prevent the stagnation of local optima. Meanwhile, a is an adaptive parameter that undergoes a linear reduction from 2 to 0 over the iteration process.

$$a = 2\left(1 - \frac{i}{T}\right) \tag{30}$$

The mathematical model mentioned above assumes that $\boldsymbol{X}_p(i)$ is known, but this assumption does not hold in a real abstract search space. In GWO, the three leader wolves are considered to have superiorities in terms of closeness to the prey. In essence, the whereabouts of the prey are estimated by the three agents: alpha (the fittest agent), beta (the second best), and delta (the third best). Consequently, the optimization process saves the top three solutions obtained thus far. The remaining search agents, including omega, follow the navigation of these leaders and update their positions based on the positions of alpha, beta, and delta in the following manner:

$$\boldsymbol{D}_\alpha = |\boldsymbol{C}_\alpha \cdot \boldsymbol{X}_\alpha(i) - \boldsymbol{X}(i)| \tag{31}$$

$$\boldsymbol{D}_\beta = |\boldsymbol{C}_\beta \cdot \boldsymbol{X}_\beta(i) - \boldsymbol{X}(i)| \tag{32}$$

$$\boldsymbol{D}_\delta = |\boldsymbol{C}_\delta \cdot \boldsymbol{X}_\delta(i) - \boldsymbol{X}(i)| \tag{33}$$

$$\boldsymbol{X}_1 = \boldsymbol{X}_\alpha(i) - \boldsymbol{A}_\alpha \cdot \boldsymbol{D}_\alpha \tag{34}$$

$$\boldsymbol{X}_2 = \boldsymbol{X}_\beta(i) - \boldsymbol{A}_\beta \cdot \boldsymbol{D}_\beta \tag{35}$$

$$\boldsymbol{X}_3 = \boldsymbol{X}_\delta(i) - \boldsymbol{A}_\delta \cdot \boldsymbol{D}_\delta \tag{36}$$

$$\boldsymbol{X}(i+1) = \frac{\boldsymbol{X}_1 + \boldsymbol{X}_2 + \boldsymbol{X}_3}{3} \tag{37}$$

Figure 4(b) demonstrates that a search agent updates its position around the estimated position of prey,[23] which is based on the leaders' positions: $\boldsymbol{X}_\alpha(i)$, $\boldsymbol{X}_\beta(i)$, and $\boldsymbol{X}_\delta(i)$.

A remarkable advantage of GWO is the reduced number of hyperparameters that need to be set in advance. Furthermore, its exceptional global search capability has promoted its utilization in tackling complex engineering challenges.[32] This study represents the first example in which GWO has been integrated with an active oscillation controller for a driveline featuring backlash.

4.2. GWO-based algorithm for controller tuning

Fig. 5 illustrates the tuning algorithm designed for the active controller with backlash management, employing the GWO algorithm as its foundation,[23] applied to both the contact and backlash modes. In subsequent discussions, the parameters updated by GWO according to Eqs. (31)-(37) are referred to as the *design variables* ($\boldsymbol{X}(i) \in \mathbb{R}^p$), while parameters dedicated to control system design are denoted as *tuning parameters*. The performance of the damping by the controller is quantified by the positive scalar loss function $J(\boldsymbol{X})$. GWO ultimately yields the alpha wolf that minimizes $J(\boldsymbol{X})$. $C_{end} \in \mathbb{N}$ represents the maximum number of iterations.

This proposed approach enables automatic fine-tuning of the active damping system, reducing the need for adjustments through trial-and-error by the designer. It optimizes both contact and backlash mode controls concurrently.

The vector $\boldsymbol{X}(i)$ holds the essential tuning parameters: Q_i, R_i, and R_i^{BL} for controlling the contact and backlash modes. Eqs. (38)-(40) describe how Q_i, R_i, and R_i^{BL} are represented in terms of the design variable $\boldsymbol{X}(i)$.

$$Q_i = |X^1(i)| \tag{38}$$

$$R_i = |X^2(i)| \tag{39}$$

$$R_i^{BL} = |X^3(i)| \tag{40}$$

$X^m(i)$ shows the mth element of $\boldsymbol{X}(i)$. $\boldsymbol{X}(i)$ is a three-dimensional vector. Eq. (41) illustrates the objective of minimizing the loss function $J(\boldsymbol{X})$.

$$J(\boldsymbol{X}) = J_i = \frac{1}{N}\left\{S_y\left(\sum_{k=1}^{N} \tilde{y}_{i,k}{}^2\right) + S_u\left(\sum_{k=1}^{N} u_{i,k}{}^2\right)\right\} \tag{41}$$

In this context, $\tilde{y}_{i,k}$ represents the error between the vibration of the vehicle and a desired reference signal at the kth sampling point during the ith iteration. $u_{i,k}$ indicates the control input at the same kth sample point during the ith iteration. N signifies the total number of sample points. S_y and S_u denote scaling factors applied to $\tilde{y}_{i,k}$ and

$u_{i,k}$, respectively. This research sets these initial conditions as $S_y = 10^0$ and $S_u = 10^{-7}$ based on the magnitude difference between the first and second terms in Eq. (41). $J(\boldsymbol{X})$ corresponds to the summation of the mean squares of both the control error and the control input.

4.3. Optimization settings and results

Table 2 indicates the settings to perform GWO shown in Eqs. (26)–(37).

Table 2. Setting for the GWO

Properties	Value
Upper bounds of design variables $[X^1(i) \quad X^2(i) \quad X^3(i)]$	$[10^2 \quad 10^2 \quad 10^2]$
Lower bounds of design variables $[X^1(i) \quad X^2(i) \quad X^3(i)]$	$-[10^2 \quad 10^{-2} \quad 10^{-2}]$
Population size	12
Number of iterations	50

In Fig. 6, the optimization results obtained by GWO are summarized. The progress of optimizing each tuning parameter is displayed in Figs. 6(a)-(c). The representative processes of minimizing the loss function are those of the alpha, beta, delta wolves, which are shown in Fig. 6(d).

In Fig. 6(d), we can see that the three loss function values J_i^{α}, J_i^{β} and J_i^{δ} are iteratively decreased during the optimization process. All the alpha, beta, and delta wolves eventually converge to the approximately same minute values owing to the exploitation ability of GWO. The quantitative optimization results are given in Table 3. For example, there is the great difference between the initial J_0^{α} and optimized J_{50}^{α} values in the alpha's loss function. This decreasing value is translated into improvement of the vibration controller's performance.

The tuning result in Table 3 was obtained as the mean of 10 trials. The total computing time of the GWO-based tuning algorithm required to optimize the control system was 18209.5926 seconds (about 5 hours). The specification of PC used for the computation is

Lenovo ThinkPad (CPU; Intel (R) Core (TM) i7-10850H CPU @ 2.70GHz, Memory; 16GB).

Because all the optimization processes by the proposed tuning algorithm are performed offline, its real-time calculation cost during the active vibration control will not be increased. In addition, introducing parallel processing calculations to average multiple trials can further reduce the computing time offline. Therefore, the proposed optimization algorithm is applicable to real vehicle driveline control.

Table 3. Tuning results based on GWO (the mean of 10 trials).

Properties	Value
Q_{50}	77.9551
R_{50}	5.4704
R_{50}^{BL}	0.00859141
J_0^{α}	0.8615
J_{50}^{α}	1.5372×10^{-5}
J_0^{β}	4.1845
J_{50}^{β}	1.5455×10^{-5}
J_0^{δ}	13.1396
J_{50}^{δ}	1.5538×10^{-5}

5. Simulation verifications

5.1. Simulation settings

This research confirms the effectiveness of the active vibration control algorithm through simulations that involve sudden, transient input variations. The validation process employs MATLAB/Simulink for this purpose. Figure 7 shows the closed-loop configuration in Simulink, which is used to validate the proposed oscillation controller.

The simulation compares the proposed approach to other controller design schemes. The first is an H_2 controller designed using GWO, but it lacks any provision for compensating for backlash. The second refers to a compensation algorithm illustrated in Fig. 2, where manually adjusting the control parameters for contact and backlash modes is not working very well.

5.2. Simulation result and discussion

Figure 8 illustrates the outcome of vibration control result (Case 0), depicting the time waveforms of vehicle oscillations in the upper graph and control inputs in the lower graph. In comparison to the scenario without any controls, denoted by the green line, all control systems effectively reduce vehicle oscillations. We can observe that the approach proposed in this research, represented by the red line, offers a superior transient response compared to the control strategies denoted by the blue and black lines. The proposed method more aggressively suppresses the oscillation, which is induced after 2.0 s. In contrast, the overshoot in the blue line indicates that the absence of backlash compensations results in poor performances. In addition, the black line also indicates the poor vibration suppression because the controller parameter tuning is not enough. As a result, it is important to have both the utilization of contact and backlash mode controllers and their appropriate adjustment. The effective dampening of vibrations, as shown by the red line, can be attributed to the capability of GWO for comprehensive searching, eliminating the need for manual tuning though trial and error.

The quantitative performance index for each result in Fig. 8 is presented in Table 4. To assess the transient response through active control, we calculated the 2-norm of the control error for each response in comparison to the desired reference signal represented by the yellow line. In Table 4, the suggested approach yields the smallest 2-norm value, indicating outstanding damping performance. Compared to “Manual design”, “No backlash control” and “No control”, the proposed method decreases the 2-norm by 54.1801%, 51.7881% and 73.7675%, respectively.

Table 4 2-norm calculated for each response in Fig. 8 (Case 0)

	Proposed method	Manual design	No backlash control	No control
2-norm	0.8486	1.8520	1.7602	3.2349

5.3. Comparison with previous backlash compensation

Regarding a backlash compensation mechanism, the proposed scheme is compared with a previous approach (hereafter referred to as *Threshold-based*). This comparison examines the efficacy owing to TDSLKF. In the previous approach, the switching between the backlash and contact modes is performed based on the setting of a threshold value for vehicle jerk, whose details can be found in the literatures.[9,14]

Figure 9(a) shows the comparative result (Case 1) where the driving condition is also changed from that of Fig. 8 to investigate the controller’s robustness. In this case, the previous approach has an adequate setting of a threshold value for vehicle jerk, thereby exhibiting the excellent transient response. The red and magenta lines almost overlap, which means that both the proposed and previous approaches provide good backlash compensation at the same level.

Figure 9(b) shows another case for the comparison: (Case 2) where setting a suitable threshold failed in the previous approach. An excessively high threshold value disrupts the transition from the backlash mode to the contact mode in *Threshold-based* system. This results in the occurrence of vibrations as well as errors from the target response.

The comparison of Figs. 9(a) and (b) indicates the necessity of an adequate setting of the jerk threshold in the previous method[14] as well as the great sensitivity to vibration suppression. However, it is not always easy because of the absence of a clear design policy and the requirement of prior information on vehicle jerk. Hence, in contrast, the proposed method based on TDSLKF, which has a more systematic manner and does not require prior setting of the jerk threshold, can be an alternative to the previous method in some situations. The transition from the backlash mode to the contact mode is facilitated by the good estimation accuracy demonstrated in Fig. 10. Fig. 10 indicates the time responses of the actual and estimated vibrations of X_B, x_G, and X_E by the blue solid and red dotted lines, respectively. The proposed method is shown to be superior by summarizing the 2-norm of each vibration response in Figs. 9(a) and (b) in Table 5. Compared to "Threshold-based compensation in Fig. 9(a)", "Threshold-based compensation in Fig. 9(b)" and "No control", the proposed method reduces the 2-norm by 0.7899%, 83.9456% and 74.9923%, respectively.

Table 5 2-norm calculated for each response in Figs. 9(a) and (b) (Cases 1 and 2)

	Proposed method	Threshold-based compensation in Fig. 9(a)	Threshold-based compensation in Fig. 9(b)	No control
2-norm	1.1055	1.1143	6.8860	4.4206

5.4. Robustness evaluation

For the active vibration controller, the sensitivity analysis (i.e., robustness evaluation) needs to be performed. This study examines the robustness to variations in the driveline parameters as well as the tolerance to measurement noise. The variation conditions are shown in Table 6.[24] The ranges of variations in driveline parameters shown in Table 6 originate from the previous literature.[24] In the previous work, the fluctuation amount was set by considering parameter variations of real-world vehicles.

Table 6 Variations in driveline parameters and observation noise

Parameter in the driveline model	Variation amount [%] (Case 3)
M_B [kg]	10
m_G [kg]	-10
M_E [kg]	-10
K_C [N/m]	10
K_D [N/m]	10
K_G [N/m]	-10
C_C [Ns/m]	-10
C_D [Ns/m]	10
C_G [Ns/m]	-10
C_{cl} [Ns/m]	10
Measurement noise (uniform distribution)	± 10

The vibration control results (Case 3) under the variations and the observation noise are shown in Fig. 11. In contrast to the deteriorated oscillations indicated by the blue and black lines, the proposed method maintains satisfactory performance, which has nearly the same level as that in Fig. 8. The red line implies the robustness to variations in the conditions of the driveline. Comparing Figs. 8 and 11 reveals that when modeling errors are introduced into the control system design, the transition from backlash mode to contact mode has a more pronounced impact on oscillations. Consequently, the presence of the red line suggests that achieving successful compensation during the backlash mode, as aimed for in the soft-landing objective, may enhance robustness. As described in the former section, the successful backlash compensation is built upon the estimation accuracy of TDSLKF. Figure 12 shows the estimation result of the time responses under the measurement noise. This test case introduces a uniform random noise of 10% to the observed output. Despite the presence of the measurement noise shown by the green line, Fig. 12 shows that the estimated time response (red dotted line) agrees well with the true one (blue solid line).

Table 7 indicates the 2-norm of each response in Fig. 11. The smallest value retained by the proposed method is regarded as the robustness against the driveline's variations. Compared to "Manual design", "No backlash control" and "No control", the 2-norm of the proposed method is reduced by 66.9290%, 58.5777% and 75.2603%, respectively.

Table 7 2-norm calculated for each response in Fig. 11 (Case 3)

	Proposed method	Manual design	No backlash control	No control
2-norm	0.7312	2.2110	1.7653	2.9556

In contrast to the existing works, this research newly demonstrated that both the suppression of driveline transient oscillations in the contact mode and the compensation for disruptive effects due to the backlash in the backlash mode can be concurrently established by the application of GWO. In addition, we found that TDSLKF can estimate the state variables of a driveline with good accuracy and its estimation is applicable to dealing with the backlash mode. Further, the robustness to variations of the driveline dynamics was revealed via numerical analysis.

The proposed approach is considered to be extensible to the application to hybrid or electric vehicle drivetrains because of its versatility and simpleness. As the ambitious extension, the basic idea may be useful not only for an automotive driveline, but also for other mechanical systems in general, where the dynamic characteristic switches discontinuously between the two modes.

In the future works, we are planning to implement the proposed control logic in a basic experimental apparatus, which has been developed reproducing the abstract driveline model. Moreover, the experiment involving a real test vehicle and the comparison with other optimization algorithms will be also needed.

6. Conclusion

The new contribution of this research is to present a GWO-based tuning algorithm of an oscillation damping control system for a vehicle driveline to ensure comfortability and drivability. This approach effectively deals with the temporary oscillations by employing an output-feedback H_2 controller while addressing the nonlinear nature of backlash through a TDSLKF-based compensation method. As one of the merits of the compensation method, we revealed that the accurate estimation of state variables by

TDSLKF allows for successful switching between different driveline control modes, specifically the contact and backlash modes. This feature results in alleviating the impact of backlash. Furthermore, another key finding is that the application of GWO can automatically determine the optimal values of parameters, which are necessary to be set for the two control modes. This finding eliminates the need for trial-and-error tuning tasks, which have been imposed when implementing controllers in real-world vehicles. Through comparative simulations using a nonlinear driveline model, the capability of the control system to reduce vibrations was confirmed, resulting in the significant finding: the suggested approach yielded the smallest 2-norm value of the vibration response, indicating outstanding damping performance. Compared to the previous backlash compensation based on the jerk threshold, the proposed active control system reduces the 2-norm of the vibration response by 83.9456%.

In the future, the suggested approach will be implemented in an abstract apparatus of a driveline mechanism for the experimental verification. Moreover, the practicability needs to be enhanced, aiming at the extension to real-world vehicles.

Declaration of conflicting interests

The authors declared no potential conflicts of interest with respect to the research, authorship, and/or publication of this article.

Funding

The authors disclosed receipt of the following financial support for the research, authorship, and/or publication of this article: This work was partially supported by the Transmission Research Association for Mobility Innovation (TRAMI) [Grant Number 23B3-01] and the Japan Society for the Promotion of Science (JSPS) KAKENHI [Grant Number 22K20396; Grant Number 23K13273].

References

1. Yücesan A, Mugan A. Development and control of an active torsional vibration damper for vehicle powertrains. *Proc Inst Mech Eng Part K J Multi-body Dyn* 2021; 235: 452–464.
2. Duc Phuc V, Tran V-T. Optimization design for multiple dynamic vibration absorbers on damped structures using equivalent linearization method. *Proc Inst Mech Eng Part K J Multi-body Dyn* 2022; 236: 41–50.
3. Raei M, Dardel M. Tuned mass damper and high static low dynamic stiffness isolator for vibration reduction of beam structure. *Proc Inst Mech Eng Part K J Multi-body Dyn* 2020; 234: 95–115.
4. Barin F, Heidari Shirazi K, M. Sedighi H. Classification of transient vibration of passenger cars powertrain. *Proc Inst Mech Eng Part K J Multi-body Dyn* 2023; 237: 442–460.
5. Vadamalu RS, Beidl C. Adaptive internal model-based harmonic control for active torsional vibration reduction. *IEEE Trans Ind Electron* 2020; 67: 3024–3032.
6. Chen X, Peng D, Hu J, et al. Adaptive torsional vibration active control for hybrid electric powertrains during start-up based on model prediction. *Proc Inst Mech Eng Part D J Automob Eng* 2021; 095440702110561.
7. Yue Y, Huang Y, Hao D, et al. Model reference adaptive LQT control for anti-jerk utilizing tire-road interaction characteristics. *Proc Inst Mech Eng Part D J Automob Eng* 2021; 235: 1670–1684.
8. Reddy P, Shahbakhti M, Ravichandran M, et al. Drivetrain clunk control via a reference governor. *IFAC-PapersOnLine* 2021; 54: 846–851.
9. Yonezawa H, Kajiwara I, Sato S, et al. Vibration control of automotive drive system with nonlinear gear backlash. *J Dyn Syst Meas Control Trans ASME* 2019; 141: 1–11.
10. Zhou Z, Guo R. A Disturbance-Observer-Based Feedforward-Feedback Control Strategy for Driveline Launch Oscillation of Hybrid Electric Vehicles

Considering Nonlinear Backlash. *IEEE Trans Veh Technol* 2022; 71: 3727–3736.
11. Zhou Z, Guo R, Liu X. A disturbance-compensation-based sliding mode control scheme on mode switching condition for hybrid electric vehicles considering nonlinear backlash and stiffness. *J Vib Control* 2022; 107754632210961.
12. Lv C, Zhang J, Li Y, et al. Mode-switching-based active control of a powertrain system with non-linear backlash and flexibility for an electric vehicle during regenerative deceleration. *Proc Inst Mech Eng Part D J Automob Eng* 2015; 229: 1429–1442.
13. Zhang J, Chai B, Lu X. Active oscillation control of electric vehicles with two-speed transmission considering nonlinear backlash. *Proc Inst Mech Eng Part K J Multi-body Dyn* 2020; 234: 116–133.
14. Yonezawa H, Yonezawa A, Kajiwara I. Efficient Tuning Scheme of Mode-Switching-Based Powertrain Oscillation Controller Considering Nonlinear Backlash. *IEEE Access* 2023; 11: 93935–93947.
15. Precup RE, David RC, Petriu EM, et al. Adaptive GSA-based optimal tuning of PI controlled servo systems with reduced process parametric sensitivity, robust stability and controller robustness. *IEEE Trans Cybern* 2014; 44: 1997–2009.
16. Oglieve CJ, Mohammadpour M, Rahnejat H. Optimisation of the vehicle transmission and the gear-shifting strategy for the minimum fuel consumption and the minimum nitrogen oxide emissions. *Proc Inst Mech Eng Part D J Automob Eng* 2017; 231: 883–899.
17. Eckert JJ, da Silva SF, Santiciolli FM, et al. Multi-speed gearbox design and shifting control optimization to minimize fuel consumption, exhaust emissions and drivetrain mechanical losses. *Mech Mach Theory* 2022; 169: 104644.
18. Eckert JJ, Barbosa TP, Silva FL, et al. Optimum fuzzy logic controller applied to a hybrid hydraulic vehicle to minimize fuel consumption and emissions. *Expert Syst Appl* 2022; 207: 117903.
19. Reddy P, Shahbakhti M, Ravichandran M, et al. Real-time predictive clunk control using a reference governor. *Control Eng Pract* 2023; 135: 105489.
20. Lin C, Sun S, Walker P, et al. Off-line optimization based active control of torsional oscillation for electric vehicle drivetrain. *Appl Sci*; 7. Epub ahead of

print 2017. DOI: 10.3390/app7121261.

21. Catenaro E, Formentin S, Corno M, et al. Auto-calibration with Stability Margins for Active Damping Control in Electric Drivelines. *2022 Eur Control Conf ECC 2022* 2022; 1186–1191.
22. Song D, Wu J, Yang D, et al. An active multiobjective real-time vibration control algorithm for parallel hybrid electric vehicle. *Proc Inst Mech Eng Part D J Automob Eng* 2022; 095440702211301.
23. Mirjalili S, Mirjalili SM, Lewis A. Grey Wolf Optimizer. *Adv Eng Softw* 2014; 69: 46–61.
24. Yonezawa H, Yonezawa A, Hatano T, et al. Fuzzy-reasoning-based robust vibration controller for drivetrain mechanism with various control input updating timings. *Mech Mach Theory* 2022; 175: 104957.
25. Yonezawa H, Kajiwara I, Nishidome C, et al. Vibration control of automotive drive system with backlash considering control period constraint. *J Adv Mech Des Syst Manuf* 2019; 13: 1–16.
26. Yonezawa H, Kajiwara I, Nishidome C, et al. Active vibration control of automobile drivetrain with backlash considering time-varying long control period. *Proc Inst Mech Eng Part D J Automob Eng* 2021; 235: 773–783.
27. Gerdes JC, Kumar V. An impact model of mechanical backlash for control system analysis. In: *Proceedings of 1995 American Control Conference - ACC'95*. American Autom Control Council, pp. 3311–3315.
28. Nordin M, Galic' J, Gutman P-O. New models for backlash and gear play. *Int J Adapt Control Signal Process* 1997; 11: 49–63.
29. Chilali M, Gahinet P. H∞ design with pole placement constraints: An LMI approach. *IEEE Trans Automat Contr* 1996; 41: 358–367.
30. Zhou K, Doyle JC, Glover K. *Robust and Optimal Control*. New Jersey: PrenticeHall, 1996.
31. Yonezawa H, Kajiwara I, Sato S, et al. Application of physical function model to state estimations of nonlinear mechanical systems. *IEEE Access* 2021; 9: 12002–12018.
32. Jenarthanan M, Ramesh S. Optimization of process conditions of Powder Mixed

Electric Discharge Machining of Nickel based Superalloy using Grey Wolf Optimizer algorithm. *Proc Inst Mech Eng Part C J Mech Eng Sci*. Epub ahead of print 7 August 2023. DOI: 10.1177/09544062231187789.

33. Liu Q, Lu H, Yonezawa H, et al. Grey-Wolf-Optimization-Algorithm-Based Tuned P-PI Cascade Controller for Dual-Ball-Screw Feed Drive Systems. *Mathematics* 2023; 11: 2259.

34. Azizi M, Talatahari S, Giaralis A. Active Vibration Control of Seismically Excited Building Structures by Upgraded Grey Wolf Optimizer. *IEEE Access* 2021; 9: 166658–166673.

35. Tripathi S, Shrivastava A, Jana KC. Self-Tuning fuzzy controller for sun-tracker system using Gray Wolf Optimization (GWO) technique. *ISA Trans* 2020; 101: 50–59.

36. Yadav S, Verma SK, Nagar SK. Optimized PID Controller for Magnetic Levitation System. *IFAC-PapersOnLine* 2016; 49: 778–782.

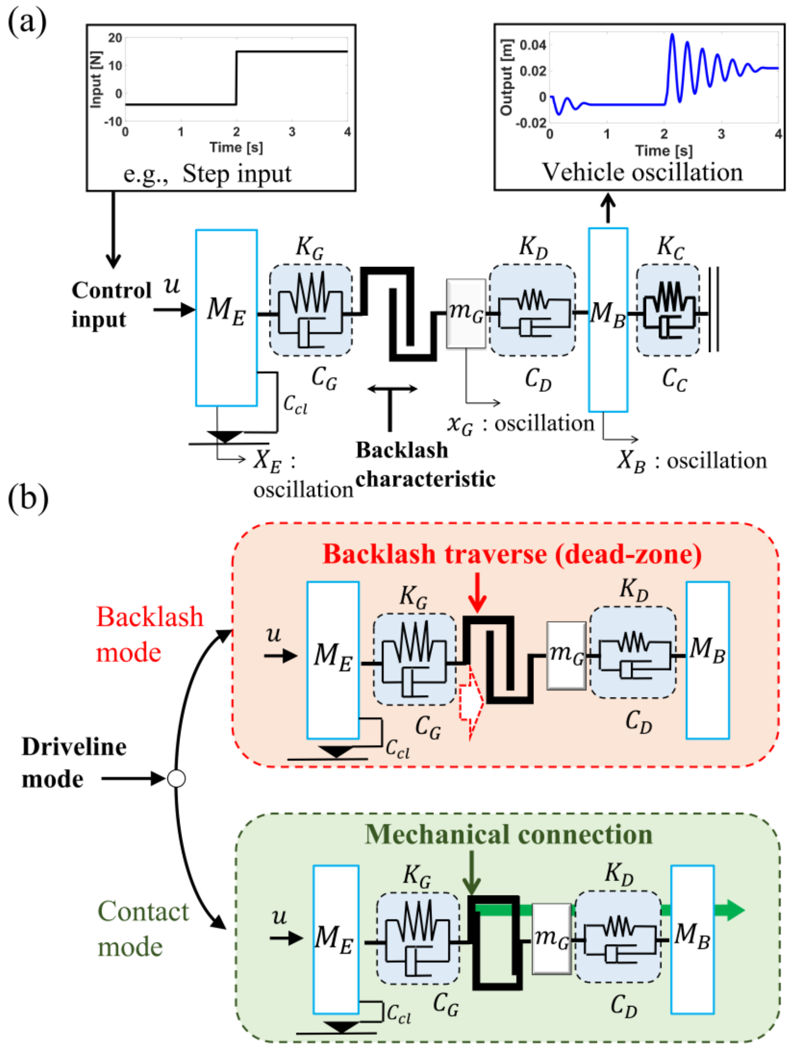

Fig. 1. Abstract drivetrain mechanism: (a) Model of mechanism (b) backlash and contact modes.

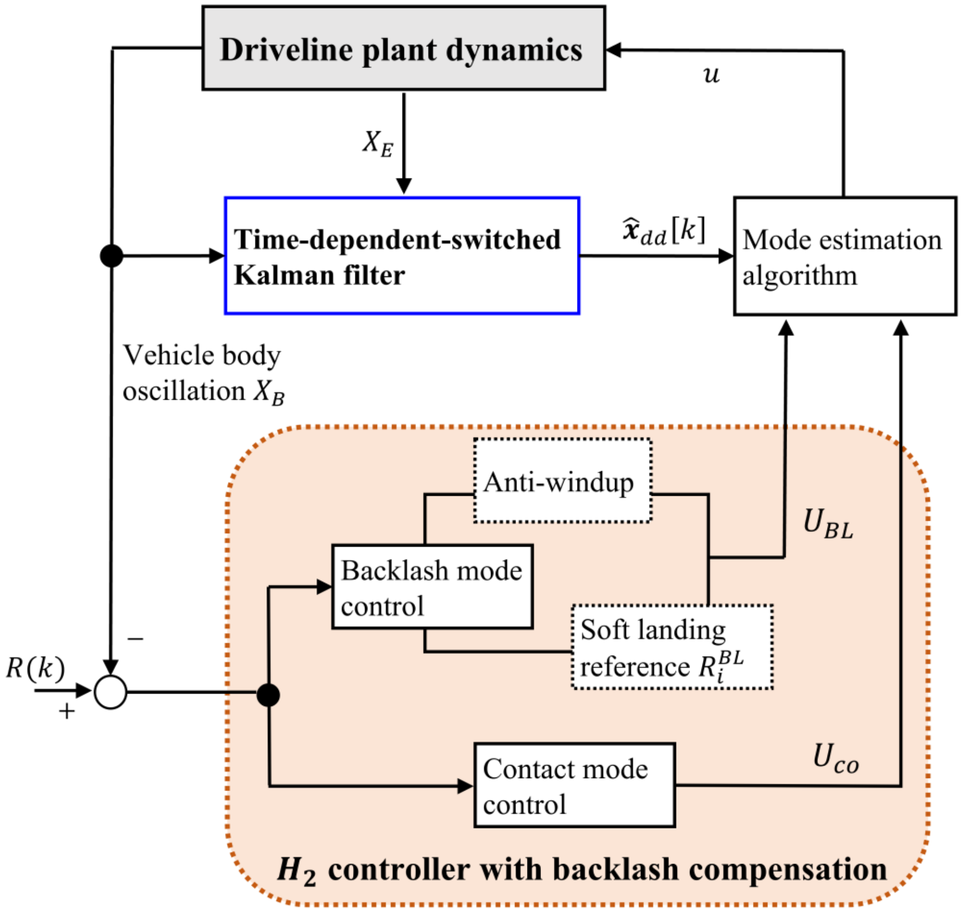

Fig. 2. Mode-switching-based drivetrain oscillation control system using TDSLKF.

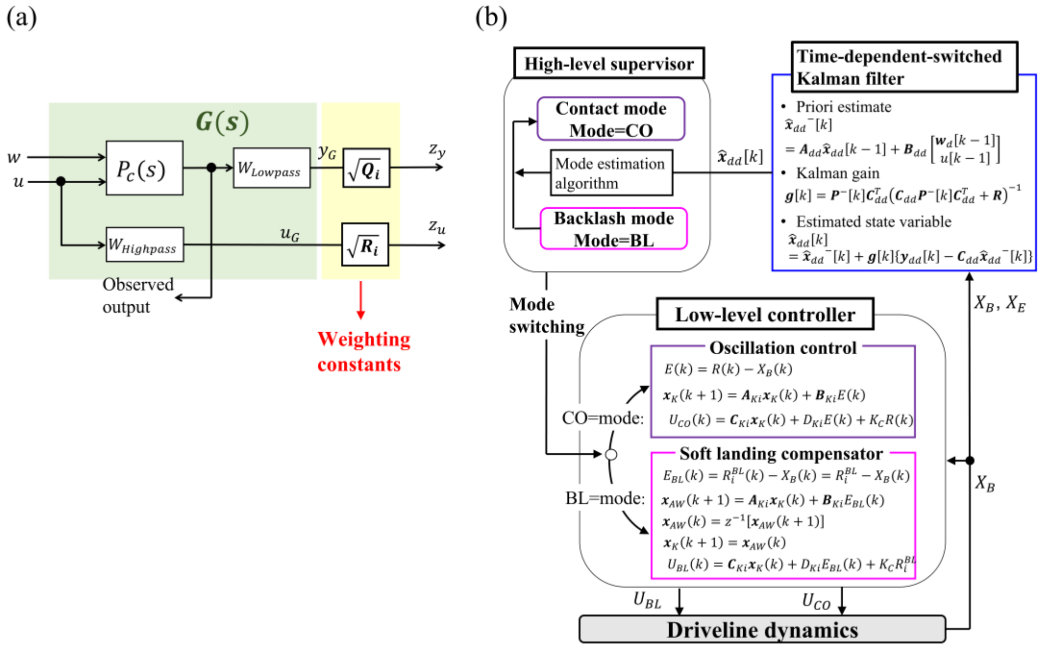

Fig. 3. Control system design: (a) generalized plant used for designing a base controller (b) mode switching structure.

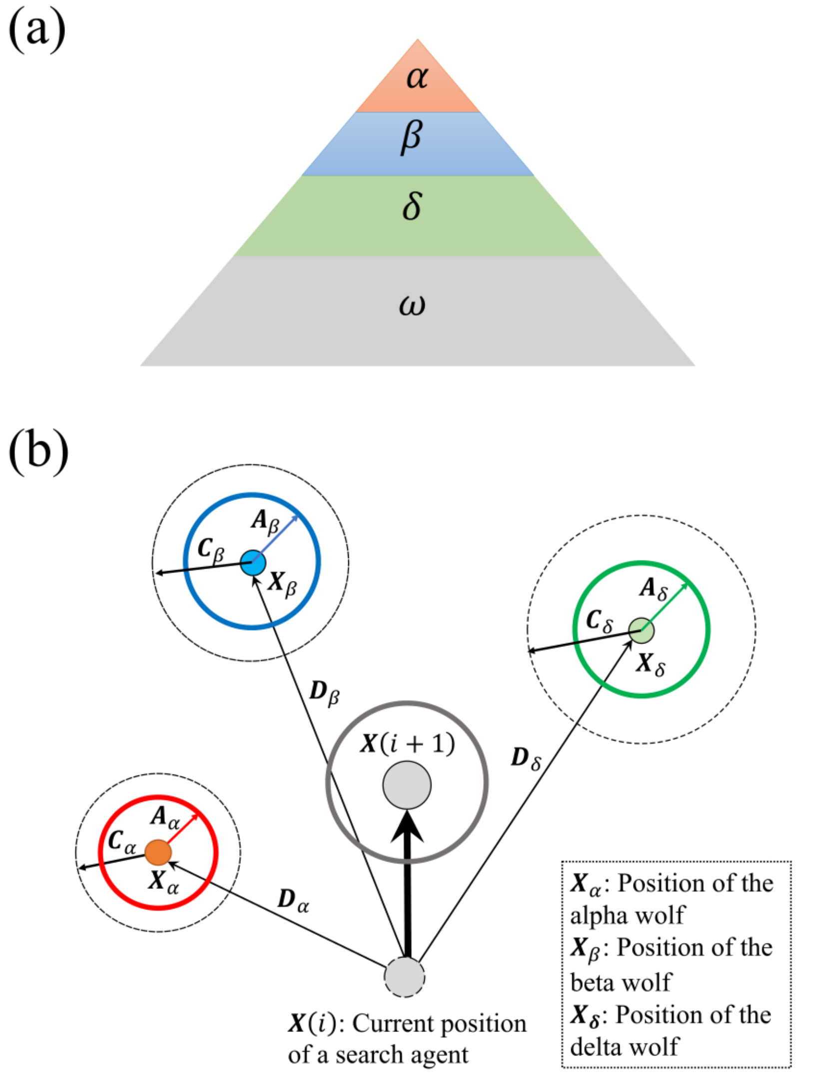

Fig. 4. Grey wolf optimizer: (a) social hierarchical structure of grey wolves in a pack (b) update of the position of each wolf.

Algorithm. Optimized tuning of CO-mode and BL-mode controllers by GWO;

Create the random population of search agents (grey wolves)
Initialize i, a, A, and C
$\boldsymbol{X}_{\alpha}$ = the best search agent
$\boldsymbol{X}_{\beta}$ = the second best search agent
$\boldsymbol{X}_{\delta}$ = the third best search agent
while $(i < C_{end})$
    for each search agent
            Update the position $\boldsymbol{X}(i)$ of the current search agent by equation (37)
    end for
    Update a, A, and C
   % Design active vibration controllers for CO-mode and BL-mode ////
    Design $(\boldsymbol{A}_{Ki}, \boldsymbol{B}_{Ki}, \boldsymbol{C}_{Ki}, D_{Ki})$ and R_i^{BL} for all search agents
   % //
    Perform vibration control simulations for all search agents
    Compute $J(\boldsymbol{X})$ as the fitness for all search agents by equation (41)
    Update $\boldsymbol{X}_{\alpha}$, $\boldsymbol{X}_{\beta}$, and $\boldsymbol{X}_{\delta}$
    $i = i + 1$
end while
Return $\boldsymbol{X}_{\alpha}$

Fig. 5. Pseudo code of the automatic tuning on the basis of the application of GWO.

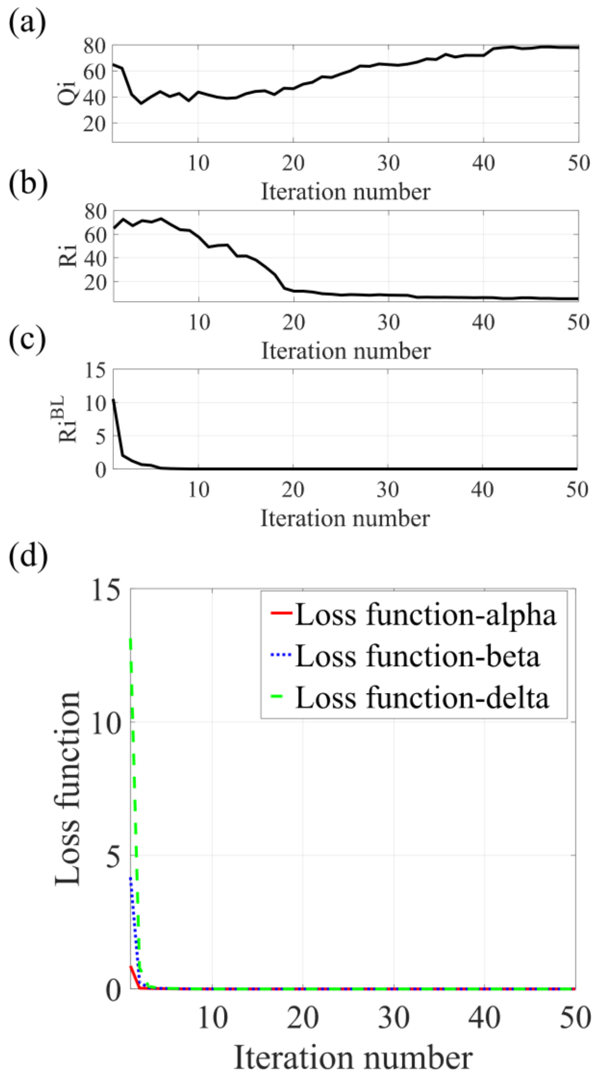

Fig. 6. Tuning results: (a) Q_i (b) R_i (c) R_i^{BL} (d) loss functions of the leader wolves.

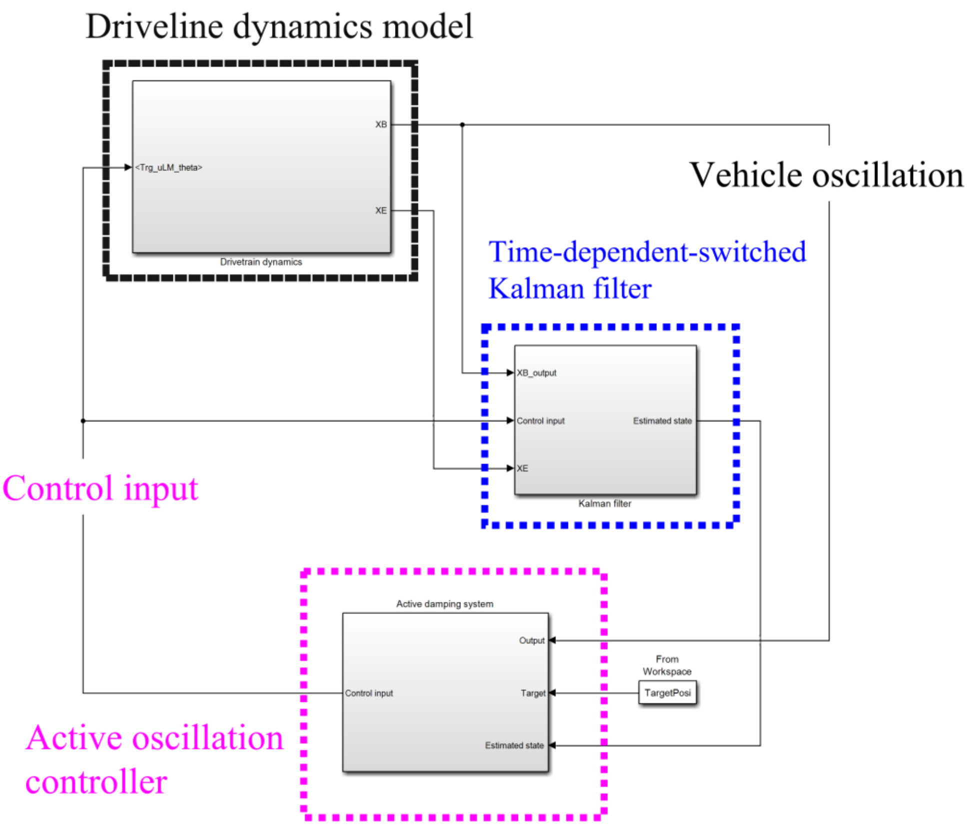

Fig. 7. Simulink structure of the proposed control system.

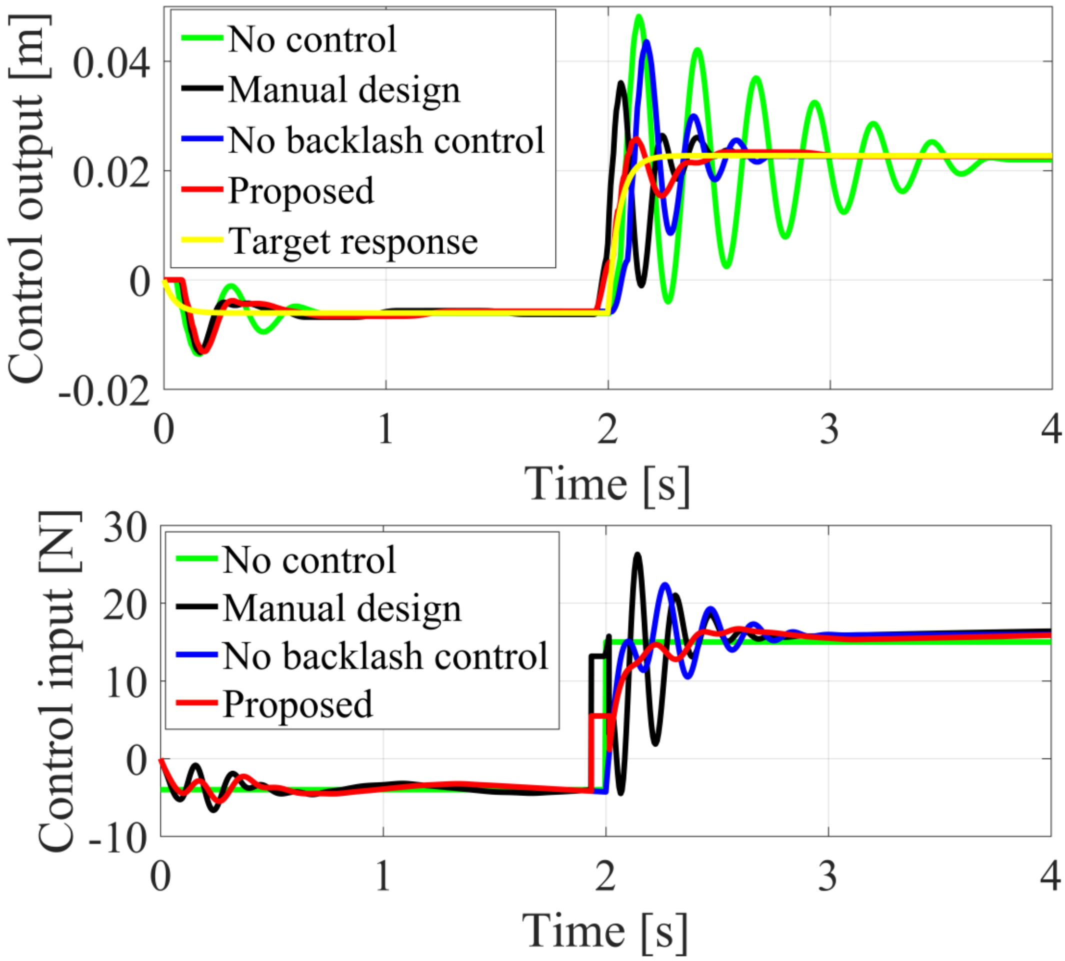

Fig. 8. Time waveforms of the control input and the vehicle oscillation in simulations (Case 0).

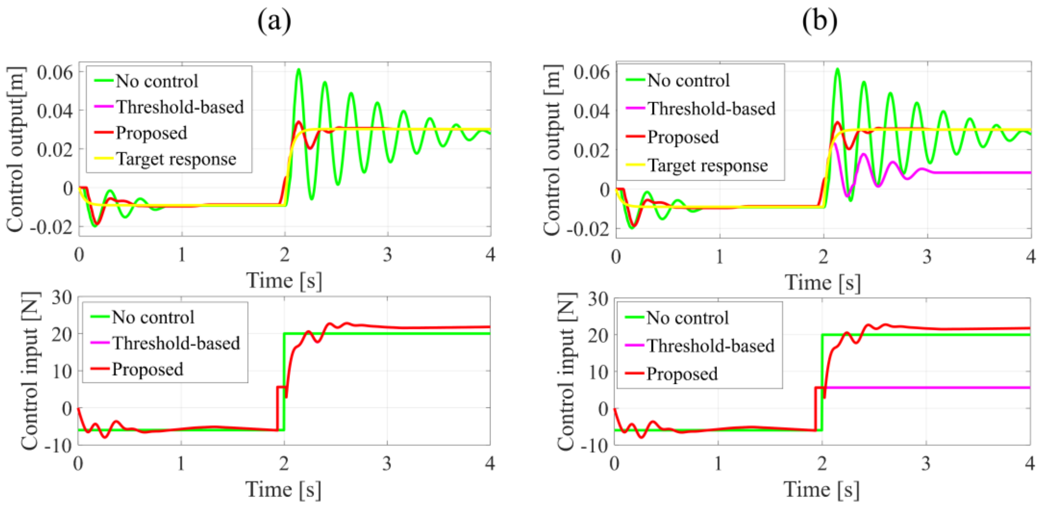

Fig. 9. Comparison results with the previous compensation mechanism: (a) case with a proper threshold value for jerk in the previous approach (b) case with an inadequate threshold value (Cases 1 and 2).

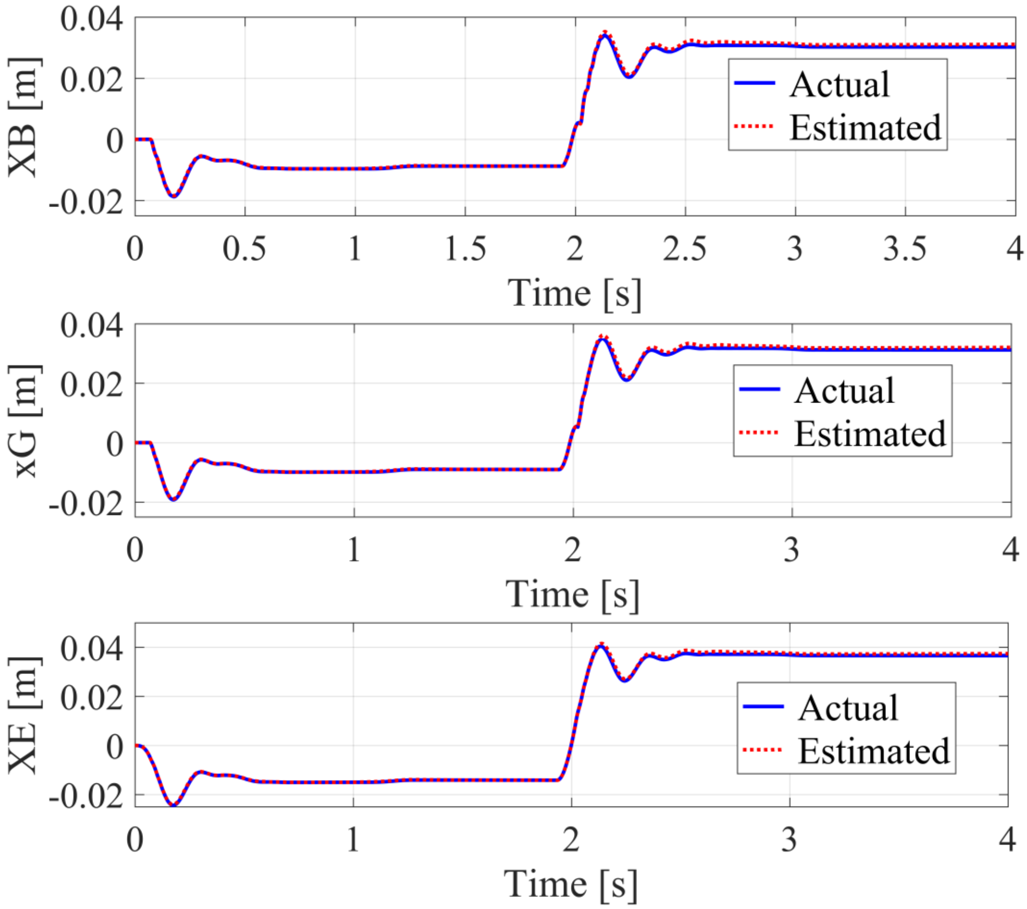

Fig. 10. Estimation result of the state variables with TDSLKF.

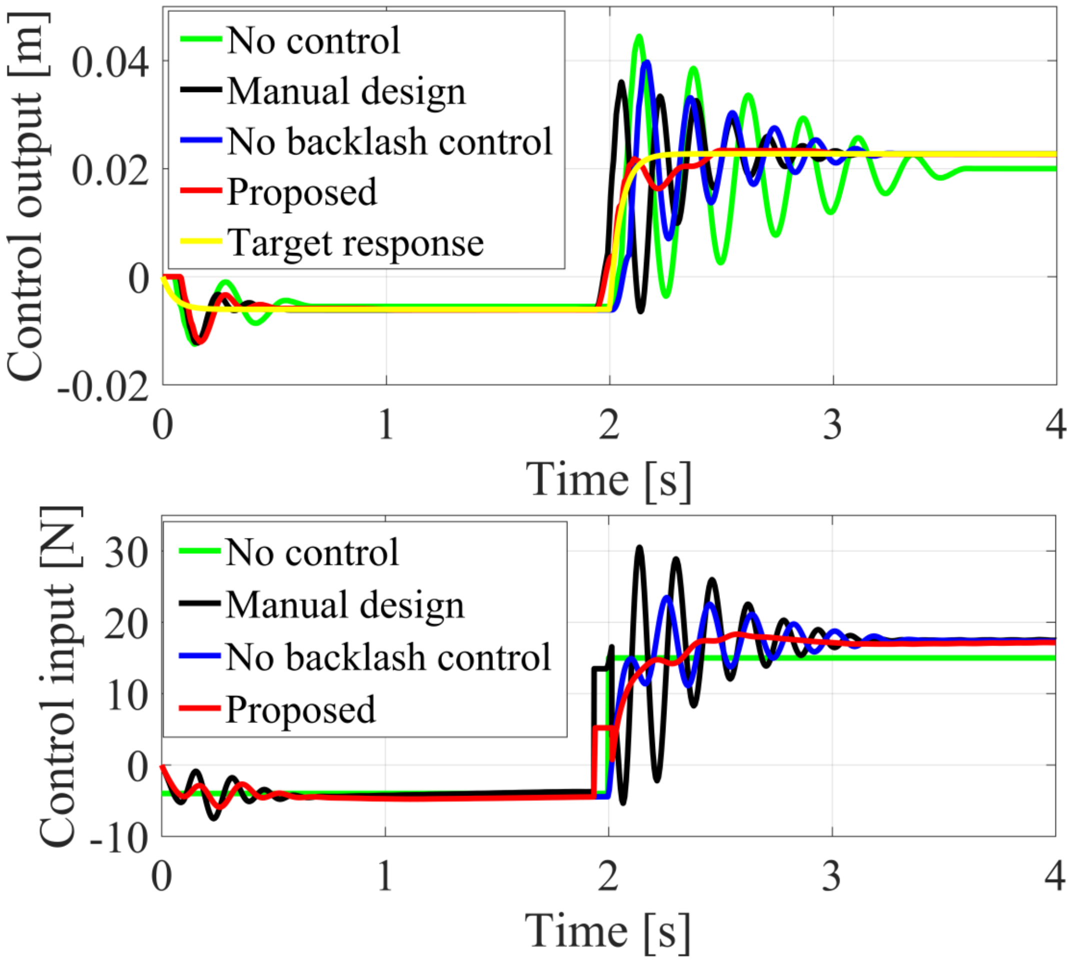

Fig. 11. Vibration control results under the parameter variations and the observation noise (Case 3).

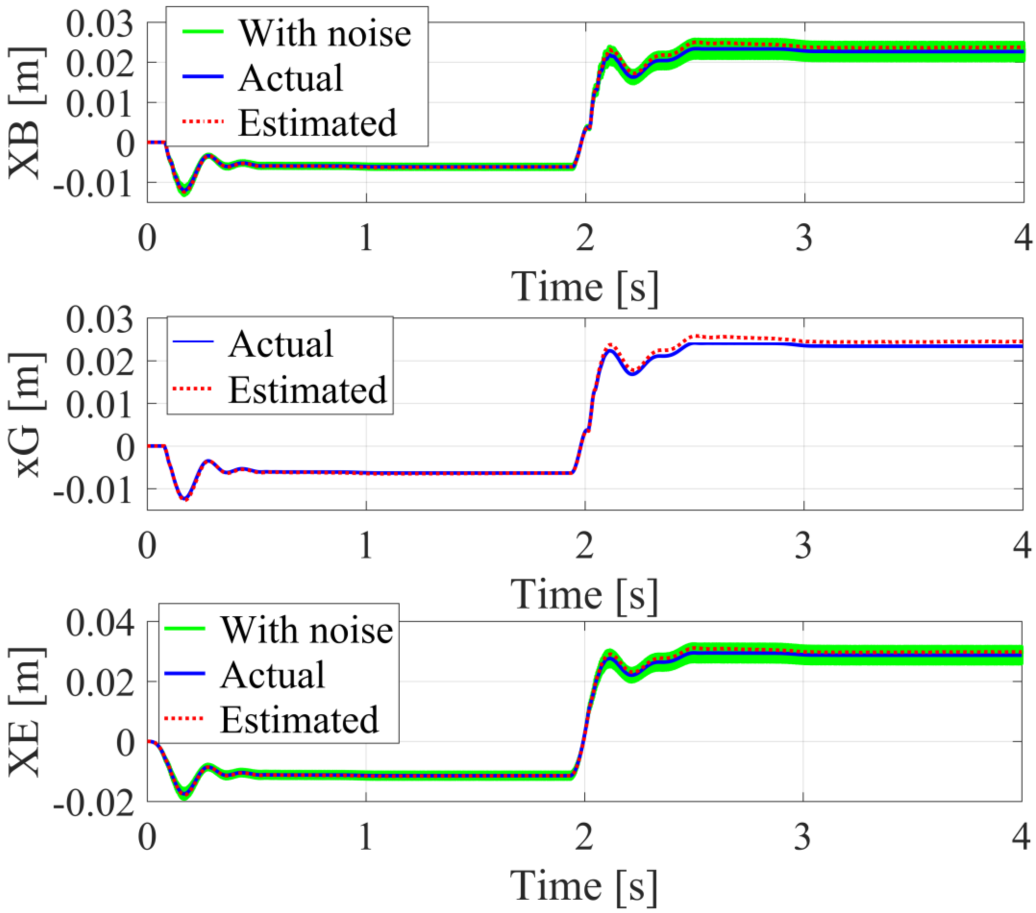

Fig. 12. Estimation result with TDSLKF under the parameter variations and the observation noise.